

Artificial Cells, Nanomedicine, and Biotechnology

An International Journal

ISSN: (Print) (Online) Journal homepage: informahealthcare.com/journals/ianb20

A new agent for contrast-enhanced intravascular ultrasound imaging in vitro: polybutylcyanoacrylate nanoparticles with drug-carrying capacity

Congying Wang, Haodong Jiang, Jia Zhu & Yunpeng Jin

To cite this article: Congying Wang, Haodong Jiang, Jia Zhu & Yunpeng Jin (2024) A new agent for contrast-enhanced intravascular ultrasound imaging in vitro: polybutylcyanoacrylate nanoparticles with drug-carrying capacity, *Artificial Cells, Nanomedicine, and Biotechnology*, 52:1, 218-228, DOI: [10.1080/21691401.2024.2334713](https://doi.org/10.1080/21691401.2024.2334713)

To link to this article: <https://doi.org/10.1080/21691401.2024.2334713>



© 2024 The Author(s). Published by Informa UK Limited, trading as Taylor & Francis Group



Published online: 22 Apr 2024.



Submit your article to this journal [↗](#)



Article views: 346



View related articles [↗](#)



View Crossmark data [↗](#)

A new agent for contrast-enhanced intravascular ultrasound imaging in vitro: polybutylcyanoacrylate nanoparticles with drug-carrying capacity

Congying Wang[†] , Haodong Jiang[†], Jia Zhu and Yunpeng Jin 

The Department of Cardiology, The Fourth Affiliated Hospital of Zhejiang University School of Medicine, Yiwu, Zhejiang, China

ABSTRACT

This study prepared and evaluated polymeric polybutylcyanoacrylate (PBCA) nanoparticles (NPs) that can be used as a new agent for contrast-enhanced intravascular ultrasound (IVUS) imaging with drug delivery capacity. The nanoformulation was successfully developed using suspension polymerisation and characterised in terms of size, size distribution, zeta potential, morphology, stability, toxicity effects, imaging effects and drug release study. The results showed that the nanoparticles were round and hollow, with a particle diameter of 215.8 ± 25.3 nm and a zeta potential of -22.2 ± 4.1 mV. In vitro experiments, the nanoparticles were safe, non-toxic, and stable in nature with the capacity to carry and release drug (ant-miR-126). Moreover, the nanoparticles can match the high-frequency probe of commercially IVUS as a contrast agent to improve the resolution of imaging (the mean echo intensity ratio in the vascular wall increased significantly from 10.89 ± 1.10 at baseline, to 24.51 ± 1.91 during injection and 43.70 ± 0.88 after injection, respectively $p < .0001$). Overall, a new nano agent with drug-carrying capacity was prepared, which can be used in combination with IVUS for simultaneous diagnosis and targeted therapy of coronary atherosclerosis.

ARTICLE HISTORY

Received 17 August 2023
Accepted 20 March 2024

KEYWORDS

Polybutylcyanoacrylate; nanoparticle; intravascular ultrasound; contrast agent; drug delivery

Introduction

Intravascular ultrasound (IVUS) is a commonly used clinical examination by intervening to deliver a tiny high-frequency ultrasound probe (25–60 MHz) to the coronary artery lesion for imaging. As a well-known medical imaging technique, IVUS plays a crucial role in the diagnosis, treatment guidance and post-treatment evaluation of coronary artery disease. However, the spatial and contrast resolution of IVUS are still relatively inadequate. This is mainly reflected in the insufficient discrimination between intravascular thrombus and hyperplastic intima, the insufficient discrimination between blood and lipid-rich plaques, the inability to clearly display images of microstructures, such as intima-media and intima-media rupture, and the inability to clearly display neoplastic trophoblastic vessels within plaques, which ultimately results in the insufficient ability to discriminate between plaque-loaded and vulnerable plaques [1, 2]. Contrast-enhanced IVUS imaging extends the capabilities of IVUS imaging by improving the contrast between the lumen and the intima of the blood vessel [3–6]. Microbubbles can be used as a contrast agent for ultrasound and enhance cellular uptake of drugs [7]. The combination of IVUS and microbubbles permit simultaneous diagnosis and treatment of coronary atherosclerosis [8]. However, the commercially available IVUS diagnostic technique is not well suited to microbubble contrast agents [9]. The resonant

frequencies of commercial microbubble contrast agents are typically <10 MHz, while transducers used in coronary IVUS typically operate at frequencies >20 MHz, making them poor excitation sources for microbubbles [10]. While this can be partially addressed by some approaches such as dual-frequency transducer, radial modulation, subharmonic or second harmonic imaging, bandwidth limitations on commercial IVUS transducers generally result in a reduction in either transmit pressure or receive sensitivity, or both [11]. The resonant frequencies of polymer-sheathed nanoparticles are higher than those of commercial microbubble contrast agents that can meet IVUS standards [12]. Moreover, the resonant frequency was observed to be higher in the smaller particle size [13]. As far, an agent that can be used to directly match commercial IVUS has not yet been reported.

Alkylcyanoacrylate (ACA) is a medical adhesive that exhibits high reactivity. In the presence of alkaline substances or a wet environment, ACA readily polymerises to form polyalkylcyanoacrylate (PACA) [14]. As a drug carrier, PACA shows great promise as a nanomaterial due to its biodegradability, favourable biocompatibility, and non-immunogenic nature. Nanoparticles (NPs) composed of PACA can carry different drugs to produce various biological effects, and can be easily modified chemically or physically to realise targeted drug delivery, which is one of the hot spots in the research of drug

CONTACT Yunpeng Jin  8013013@zju.edu.cn  The Department of Cardiology, The Fourth Affiliated Hospital of Zhejiang University School of Medicine, N1 Shangcheng Road, Yiwu, Zhejiang, China

[†]These authors contributed equally to this work.

© 2024 The Author(s). Published by Informa UK Limited, trading as Taylor & Francis Group

This is an Open Access article distributed under the terms of the Creative Commons Attribution-NonCommercial License (<http://creativecommons.org/licenses/by-nc/4.0/>), which permits unrestricted non-commercial use, distribution, and reproduction in any medium, provided the original work is properly cited. The terms on which this article has been published allow the posting of the Accepted Manuscript in a repository by the author(s) or with their consent.

delivery system at present. Commonly used monomers of ACA are methylcyanoacrylate (MCA), ethylcyanoacrylate (ECA), butylcyanoacrylate (BCA), isobutylcyanoacrylate (IBCA), etc. Since the degradation rate of PACA in vivo is inversely proportional to the length of alkyl chain, and the cytotoxicity decreases with the chain lengthening, polybutylcyanoacrylate (PBCA) is the most widely and intensively researched nanomaterial. PBCA stands out from other nanoparticle materials with its high adsorption, low toxicity and excellent biodegradability. Its strong modifiability also allows it to be modified by different substances, thus obtaining different physicochemical properties and targeting functions, which greatly broadens its scope of use [15]. In this study, polymeric PBCA NPs were synthesised and assessed across various dimensions. The NPs can be used as a new agent for contrast-enhanced IVUS imaging with drug transport capacity.

Materials and methods

Materials

Several important materials were used for the research. Specifically, ant-miR-126 and BCA were purchased from GenePharma (Suzhou, China) and Macklin (Shanghai, China), respectively. Trehalose and Tween 80 were obtained from Solarbio (Beijing, China). Poloxamer 188, also known as Pluronic F68 or poly (ethylene glycol)-block-poly (propylene glycol)-block-poly (ethylene glycol) was purchased from Aladdin (Shanghai, China). Phosphate-buffered saline (PBS) was purchased from KeyGEN BioTECH (Jiangsu, China). Primary rat aortic endothelial cells and primary endothelial cell culture system were supplied by iCell Bioscience Inc. (Shanghai, China). Three porcine aortas were excised from three normal male domestic pigs (4- or 5-month-old) with a mean bodyweight of 81 ± 4 kg at the animal laboratories, Zhejiang University, China. Furthermore, ox-LDL was obtained from YiyuanBiotech (Guangzhou, China). All other materials are analytical-grade.

It should be noted that all reagents and compounds were used as received without further purification unless specified otherwise. All the equipment was calibrated and operated according to the manufacturer's instructions. All experiments were repeated at least three times. All research complied with the Guide for the Care and Use of Laboratory Animals and were approved in advance by Zhejiang University Ethics Committee (Approval No.: ZJU15781).

Preparation of IVUS-resistant ant-miR-126 PBCA NPs

This study presents a methodology for the development of IVUS-resistant ant-miR-126 PBCA NPs, utilising a suspension polymerisation technique followed by sonication centrifugation. Initially, an IVUS probe underwent sonication for one minute within a 50ml test tube. Electron microscopy was used to assess the probe's integrity, providing insight into the ideal parameters for creating IVUS-resistant structures. The optimal method of preparation involved three primary steps:

The first step entailed the creation of Drug Aqueous Solution I, where the RNA drug 2 OD and 0.5g of BCA were

dissolved in 20ml of 0.01 M HCl. This was followed by the second step, preparing Drug Aqueous Solution II, which required dissolving 1% w/v Poloxamer 188 in 20ml of 0.01 M HCl.

Subsequently, in the third step, Drug Aqueous Solution I was incorporated into Drug Aqueous Solution II. This combined solution underwent shearing using a high-speed disperser (S10 type, SCIENTZ, Ningbo, China) for 90s at a rate of 8,000–15,000rpm. Then, the solution was stirred at 600–800rpm for 4h on a heatable magnetic stirrer (MS-H280-pro, DLAB, Beijing, China). The polymerisation process was halted by neutralisation with 0.1M NaOH, which yielded a pH of 6.7–7.0. An additional hour of stirring followed. Centrifugation of the solution at 15,000rpm for 60min allowed for separation, with the supernatant washed three times with ultrapure water, involving centrifugation for 10min at 15,000rpm for each washing. The resulting NPs were then resuspended in 1% w/v trehalose dihydrate and freeze-dried, ultimately providing drug-loaded PBCA NPs. A crucial point in the third step was pH monitoring post-polymerisation using precision pH strips. If the solution turned pink (indicative of a high pH), it was adjusted to a pH of 6.7–7.0 using HCl. Finally, the IVUS-resistant blank PBCA NPs (no drugs carried) were synthesised following the above-mentioned protocol, with the only exception being the omission of ant-miR-126 (2 OD) from the medium. The experiment involves ultra-micro spectrophotometer (nanophotometer np80, Implen, Germany) and pure water metre (HHitech, Shanghai, China).

In vitro characterization of IVUS-compatible PBCA NPs loaded with ant-miR-126

Morphological observation of blank PBCA NPs and ant-miR-126 loaded PBCA NPs

A 2ml sample of ant-miR-126 loaded PBCA NPs was washed three times with 0.1M PBS (pH 7.4) and centrifuged at 1,500rpm for 15min. The supernatant was discarded, and the NPs were fixed with 2.5% glutaraldehyde phosphate buffer for 1h. Subsequently, the NPs were fixed with 1% osmium tetroxide fixative for approximately 2h, followed by three washes with 0.1M phosphate buffer or distilled water, each lasting 5min. The NPs were dehydrated using a gradient ethanol series, including 30%, 50%, 70%, and 90% ethanol for 10–15min each. The NPs were then infiltrated with a 1:1 mixture of acetone embedding medium for 1–2h. Polymerisation was carried out at 37°C for 12h, followed by an additional 24–36h at 60°C. The samples were sectioned, stained with saturated uranyl acetate for 30min and lead citrate for 5–8min, and observed and photographed using transmission electron microscopy (JEM-1230(80KV), JEOL, Japan) and scanning electron microscopy (Quanta250, FEI, USA). The same procedure was performed on blank PBCA NPs, excluding the addition of ant-miR-126 to the culture medium.

Size, size distribution, zeta potential of blank NPs and ant-miR-126 loaded PBCA NPs

A 2ml sample of ant-miR-126 loaded PBCA NPs was centrifuged and washed three times with PBS at room temperature at 1,500rpm for 5min. The sample was then transferred to a

cuvette, and the particle size and zeta potential were measured using a zeta potential and particle size analyser (90Plus/BI.MAS Brookhaven, USA). The same procedure was performed on blank PBCA NPs, excluding the addition of ant-miR-126 to the culture medium.

Stability of blank NPs and ant-miR-126 loaded PBCA NPs

To evaluate the stability of blank NPs, three 0.1 ml samples of blank PBCA NPs were washed three times with PBS at room temperature at 1,500 rpm for 5 min, and stored at 4°C. After 24 h, 48 h, 72 h, and 7 days, observe the NPs and capture images using transmission electron microscopy to compare the time of NPs rupture. The same method as above is used to measure the stability of ant-miR-126 loaded PBCA NPs.

Toxicity assessment of blank NPs and ant-miR-126 loaded PBCA NPs

Primary rat aortic endothelial cells (after 50 µg/mL ox-LDL treatment for 24 h) were cultured in 96-well plates at a density of 5,000 cells/well. Treatment with addition of PBCA NPs (0, 0.1, 0.5, 1, 2, 4, 10 mg/ml) was carried out according to experimental grouping, and the cells in 96-well plates to be tested were replaced with the same medium at 100 µ per well. 10 µl of CCK8 reagent was added to each well, and the cell viability was observed after 48 h of incubation in the incubator.

In vitro experiments of ant-miR-126-loaded PBCA NPs for IVUS-targeted drug delivery and enhancing its resolution

Three porcine aortas were excised from healthy pigs as experimental vessels (all without significant plaque), injected with fresh blood, and imaged with IVUS. First, record the initial image. Then, 2 ml of PBCA NPs were injected through a guide catheter near the imaging catheter while keeping the imaging catheter in a fixed position. Images were observed and recorded after an acute IVUS operation. After waiting for 1 min, the IVUS procedure was repeated, and images were observed. Ultimately, the acquired images were subjected to a comparative and analytical examination. The OptiCross™ Intravascular Ultrasound catheter (40 MHz, Boston Scientific, USA) with a mechanical rotating transducer was used to perform IVUS.

Therapeutic efficacy of IVUS-compatible ant-miR-126 loaded PBCA NPs

Primary rat aortic endothelial cells were cultured and identified using von Willebrand factor (vWF) immunofluorescent staining. The experiment included a normal group, a drug solution group, a blank PBCA NPs group, and an ant-miR-126 loaded PBCA NPs group (drug loading content of 0.5 OD). The experimental procedure involved the preparation of drug solutions, PBCA NPs, and ant-miR-126 loaded PBCA NPs following the steps described in this paper. The extracts were

obtained by sonication for 1 min and filtration, and then the extracts were incubated with the cells for 16 h. The expression of miR-126 (miR-126-3p) in the cells was detected using quantitative PCR (qPCR) [16].

Cellular injury models were established by inducing endothelial cell damage with ox-LDL (50 µg/ml) for 24 h. In the drug group, pre-treatment with drug-loaded PBCA NPs was performed before modelling (specific dosage and duration determined in pre-experiments). Oil red O staining and biochemical assays were used to determine the levels of total cholesterol (TC) and free cholesterol (FC) in the cells, indicating the presence of injury. After 24 h of injury, cell viability was measured using CCK-8 assay, apoptosis was analysed by flow cytometry, nitric oxide (NO) levels and lactate dehydrogenase (LDH) leakage were measured using enzyme linked immunosorbent assay (ELISA) [17], and the expression of miR-126 in the cells was detected using qPCR.

Analysis of contrast-enhanced sequences

All recorded sequences were analysed using automated algorithms to detect, quantify, and visualise perfusion in contrast-enhanced image sequences. In brief, a human operator delineated the inner and outer boundaries of the subset and defined the region of interest on the first frame of that subset. For example, to monitor plaques, the operator provided luminal-boundary contours as well as contours indicating the intima/media interface. The images underwent contrast enhancement, resulting in noticeable changes in specific regions. These changes were then measured and displayed in a quantified and visual manner. To quantify this enhancement, the greyscale levels of the difference images on the region of interest (ROI) were averaged to generate the statistic of mean enhancement in ROI (MEIR).

Statistical analyses

Data were summarised using simple descriptive statistics. Unless otherwise stated, continuous variables were expressed as mean and standard deviation. The quantification of enhancement after microbubble injection was represented as the percentage of enhancement compared to the baseline image before injection (% ΔMEIR) and was evaluated using parametric or non-parametric analyses as appropriate. For selected regions (vascular wall), a paired-sample Student's *t*-test was used to compare the statistic Δ-MEIR values. The changes in enhancement after NPs injection between different vascular regions (vascular wall) were compared using independent-sample *t*-tests. A *p*-value of less than .05 was considered statistically significant.

Results and discussion

Preparation of PBCA NPs and ant-miR-126 loaded PBCA NPs

PBCA NPs and ant-miR-126 loaded PBCA NPs were successfully synthesised using suspension polymerisation and

acoustic centrifugation techniques. The BCA monomer exhibits high self-polymerisation activity and polymerise itself into PBCA NPs in acidic medium without requiring energy input, and exhibits high stability, making the preparation of PBCA relatively simple [18]. Additionally, PBCA NPs have a higher resonant frequency, making them more suitable for the operating frequencies of commercial IVUS transducers. The utilisation of PBCA NPs as contrast agents can enhance the contrast between the lumen and intima of blood vessels, thereby improving the resolution and diagnostic capabilities of IVUS imaging. Currently, there is extensive research focused on nanoscale synthetic polymers as drug carriers, which offer enhanced safety and reliability compared to viral vectors. These polymers provide an excellent approach for controlled release and targeted delivery of drugs [19, 20].

Size, size distribution, and zeta potential of NPs

Particles with a diameter smaller than 700 nm possess the capability to traverse the interstices within the endothelium

of blood vessels with plaque burden and manifest their physiological influences [21]. Using the zeta potential and particle size analyser (90Plus/BI-MAS Brookhaven, USA), it was determined that the PBCA NPs and ant-miR-126 loaded PBCA NPs (Figure 1) met the required specifications in this investigation. The average particle size of PBCA NPs is about 215.8 ± 25.3 nm, and the average particle size of ant-miR loaded PBCA NPs is about 427.5 ± 80.1 nm, both particle sizes are concentrated. The results also showed that PBCA NPs and ant-miR-126 loaded PBCA NPs were formed with stable negative zeta potential (Figure 2). The zeta potential of PBCA NPs is measured to be -22.2 ± 4.1 mV, while the zeta potential of ant-miR loaded PBCA NPs is determined to be -22.7 ± 7.2 mV.

Evaluation of the NPs' morphology

Whether loaded with drugs or not, electron micrographs of NPs show smooth spherical structures without apparent breakpoints or pitting (Figures 3–5). The good morphology exhibited by the NPs laid the foundation for further experiments.

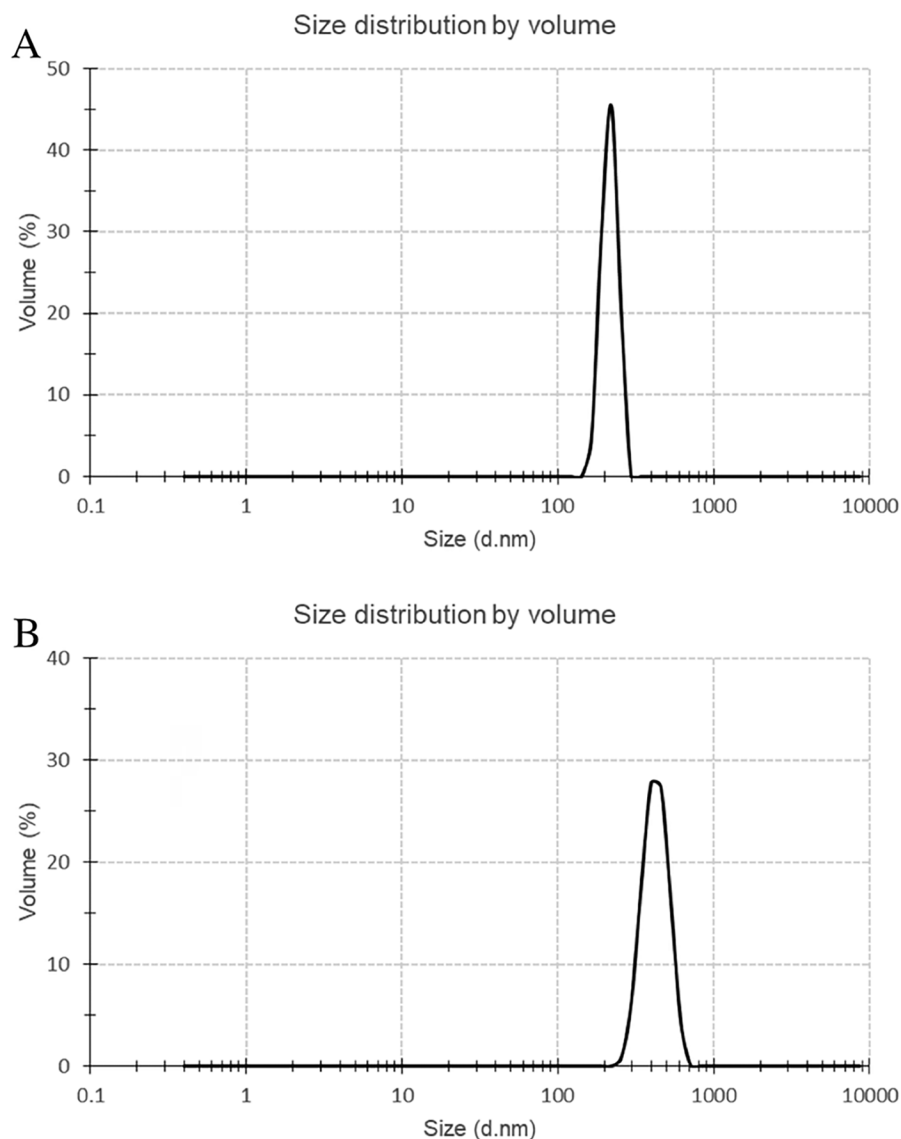


Figure 1. The size, size distribution of (A) blank polybutylcyanoacrylate (PBCA) nanoparticles (NPs) and (B) ant-miR-126 loaded PBCA NPs.

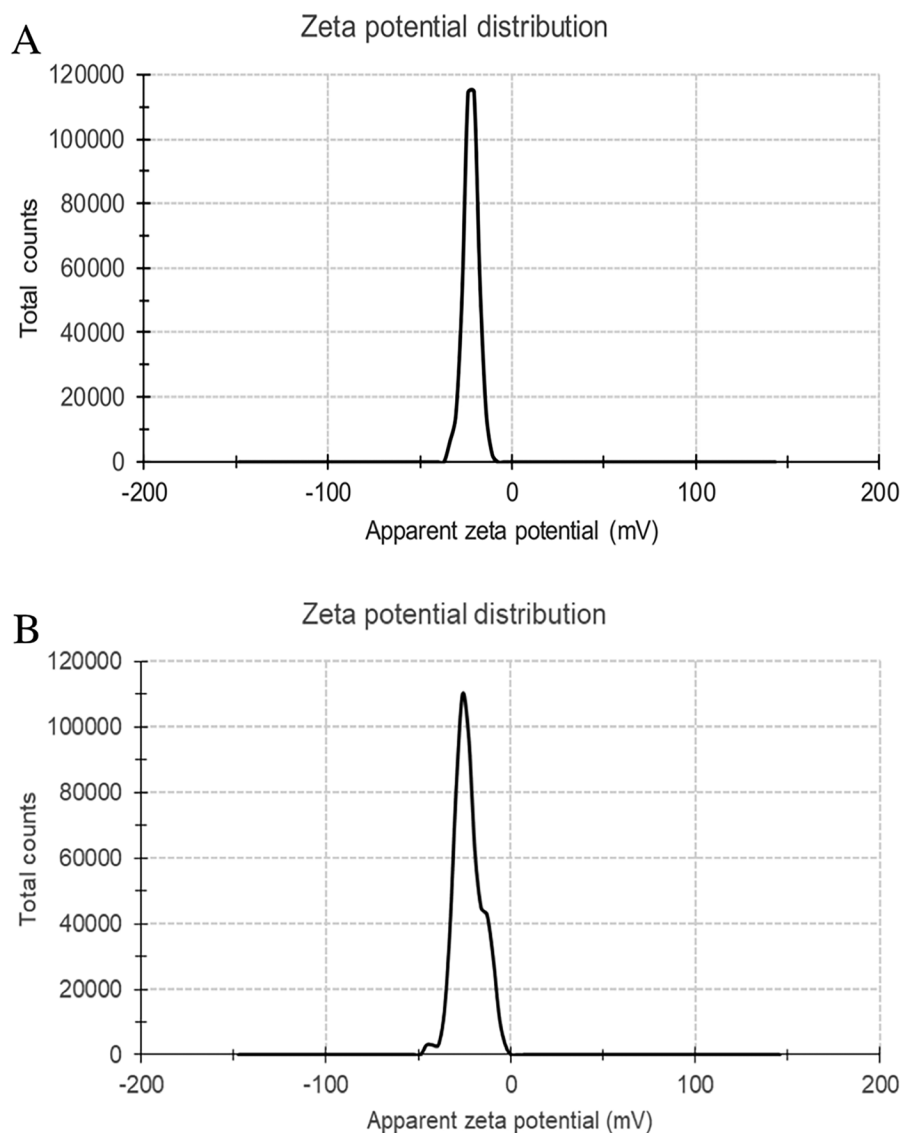


Figure 2. Zeta potential distribution of (A) blank PBCA NPs and (B) ant-miR-126 loaded PBCA NPs.

Evaluation of the NPs' stability

Prior research has demonstrated that PBCA NPs have reasonable stability as they are stable polymer-based nanocarriers. The aforementioned phenomenon can be ascribed to the inherent rigidity of their matrix or shell, which enables them to sustain their structural integrity for a prolonged duration [22–24]. The study revealed that both the blank and ant-miR-126 loaded NPs exhibited structural integrity without substantial breakage following a 7-day storage period at a temperature of 4°C. This finding suggests that the NPs possess relatively good stability.

Evaluation of ant-miR-126 loading efficiency

An assessment of the loading efficiency was not conducted as the loaded ant-miR-126 could not be detected. Given the potential impact of enhanced loading efficiency on treatment effectiveness, future studies can focus on addressing this particular issue.

Cytotoxicity studies

The results have demonstrated that the primary rat aortic endothelial cells are able to survive even in the presence of PBCA NPs, indicating low toxicity of the NPs (Figure 6). Therefore, NPs can be considered safe and non-toxic, suitable for further research and potential clinical applications. In short, it can be stated that the PBCA NPs exhibit favourable biocompatibility, thereby ensuring their potential for extensive investigation and utilisation within the human body in forthcoming research and applications. However, one limitation in particular for the cardiovascular field is reported off-target effects in organ systems, in which systemically injected miRNA-loaded PBCA NPs accumulate to a much higher extent than the targeted heart or vessel wall [25, 26]. It has been shown that a reduction in miR-126 levels decreases anti-tumor immune responses to some extent [27]. Therefore, in this study, the combination of IVUS and PBCA NPs is expected to enable targeted drug delivery and avoid undesired off-target effects. Future work is necessary to

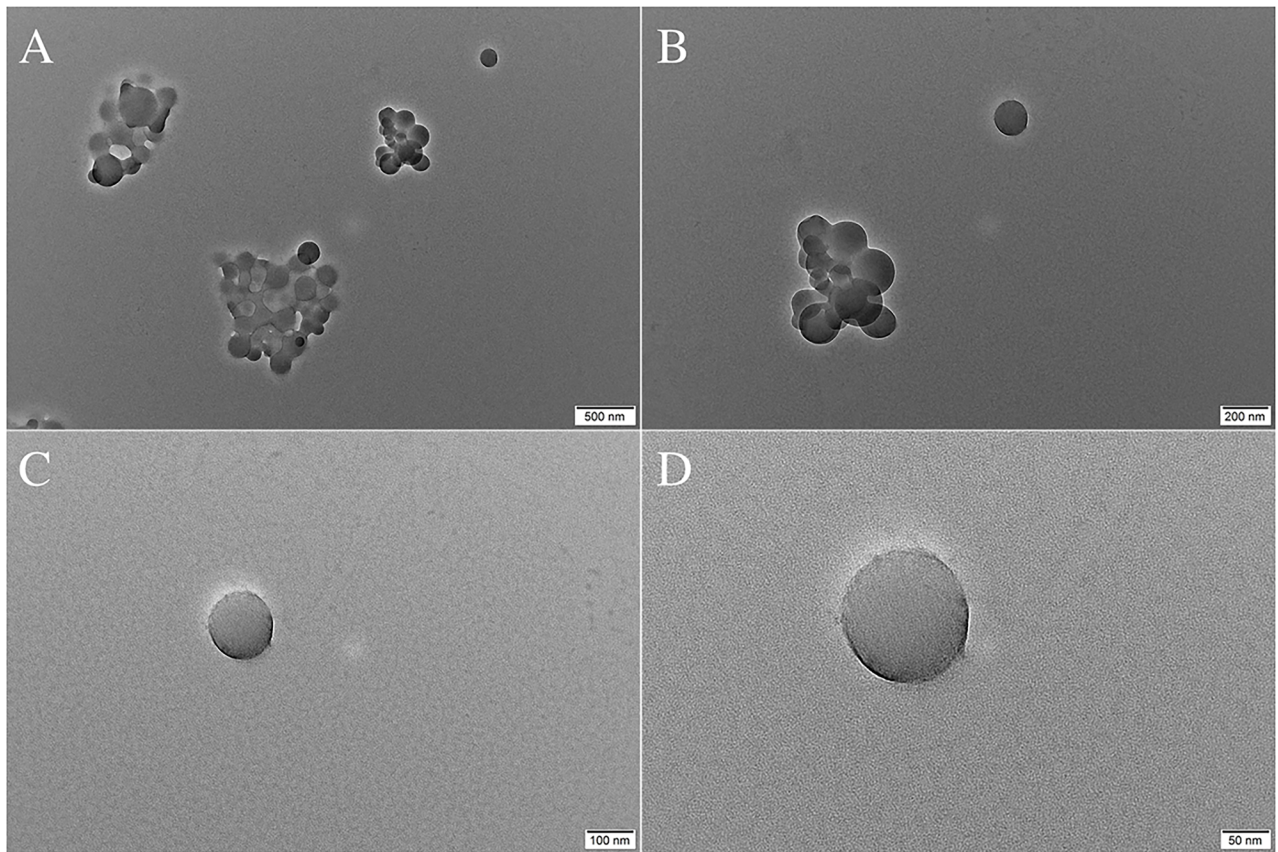


Figure 3. Morphology of blank PBCA NPs under transmission electron microscopy.

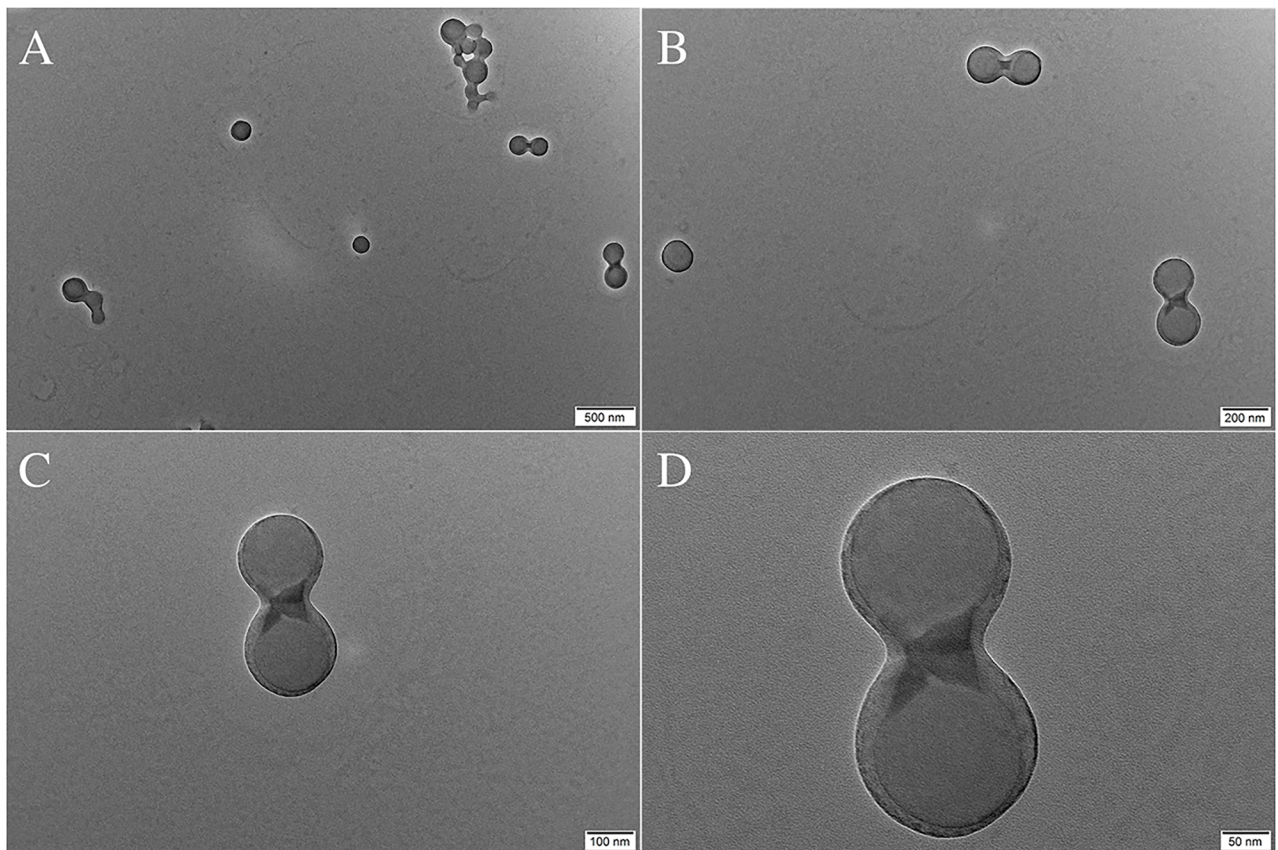


Figure 4. Morphology of ant-miR-126 loaded PBCA NPs under transmission electron microscopy.

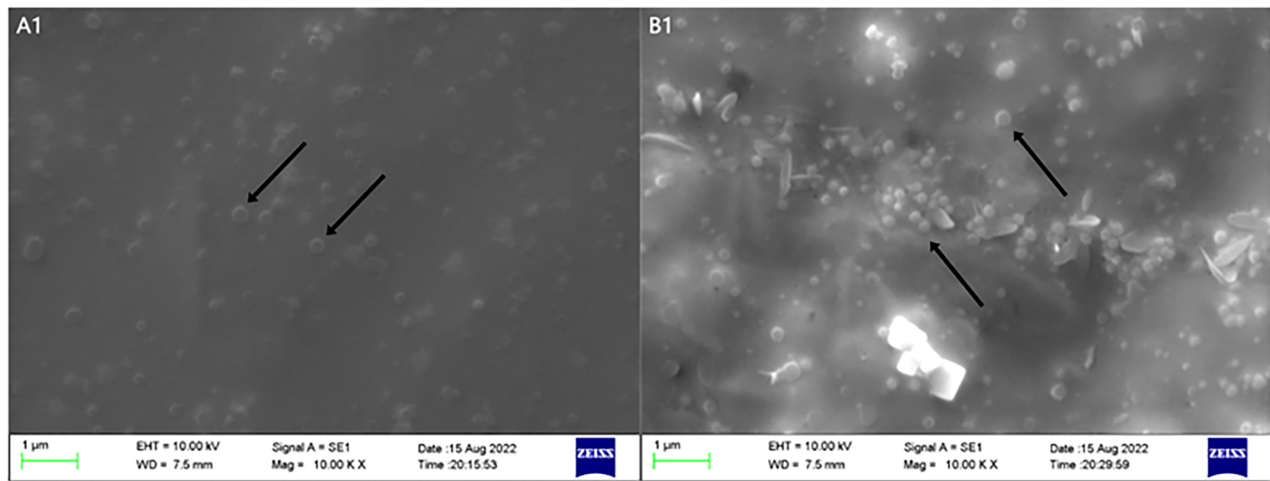


Figure 5. Scanning electron microscopy schematic diagram of blank PBCA NPs extraction solution (A1), ant-miR-126 loaded PBCA NPs extraction solution (B1). Smooth and full NPs can be seen, for example, where these arrows indicate.

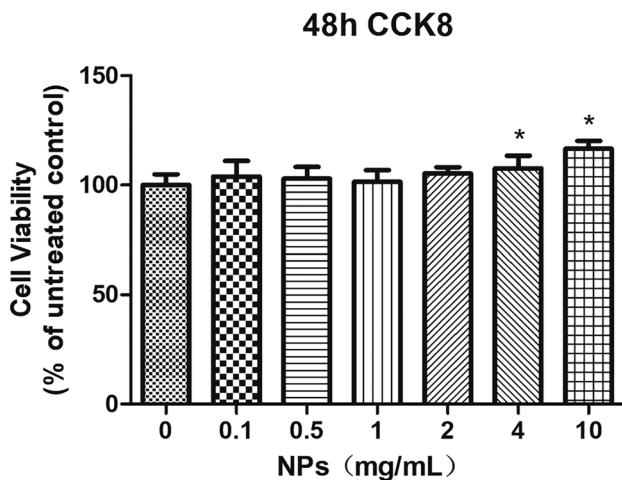


Figure 6. Schematic diagram of toxicity testing of PBCA NPs drug carrier. * indicates $p < .05$ compared with the control group.

investigate targeting efficiency and off-target effects in in vitro experiments.

In vitro for contrast-enhanced intravascular ultrasound imaging

The challenge of combining contrast agents for ultrasound imaging (e.g. ultrasound contrast agents) with IVUS and their lack of therapeutic effects has not been adequately resolved at present. Numerous studies have attempted to solve the above issues by optimising imaging analysis methods [3–5], improving ultrasound devices [28, 29], and developing novel ultrasound contrast agents that can be directly combined with existing IVUS devices and contain drugs [12]. Despite the progress made, there are still problems, such as low imaging rates, difficulties in commercialisation and widespread adoption, and a low safety profile. In addition, drug loading, controlled drug release, and targeted delivery capabilities have achieved some success in clinical applications for NPs [18–20].

The current investigation showcases the impact of NPs by means of a quantitative analysis of greyscale values in IVUS imaging. When analysing the images before and after enhancement, the qualitative analysis of the enhanced region can be observed in different vessel wall areas (Figure 7). After quantitative analysis, the echo enhancement of vessel wall regions was statistically significant (Table 1, Figure 8). After injection of PBCA NPs, the MEIR in the vessel wall increased significantly (10.89 ± 1.10 at baseline, 24.51 ± 1.91 during injection, and 43.70 ± 0.88 after injection, respectively, $p < .0001$). The MEIR value is equivalent to the difference between the average gray value of the ROI (the average gray value of the vessel wall) and the overall average gray value (the average gray value of the vessel wall and the vessel lumen).

The qualitative analysis of the pre- and post-injection images showed a gradual decrease in signal in the luminal region of the vessel and a significant improvement in the vessel wall region, as depicted in Figure 7. Quantitatively, the vessel wall MEIR showed a significant increase after injection of PBCA NPs. In this in vitro setting, it was observed that PBCA NPs entered the vessel lumen first after intravenous administration and became visible in the vessel wall after a delay of 5 to 10s. Meanwhile, the prepared NPs can be detected by the high-frequency IVUS, which also proves that the NPs have relatively higher resonant frequencies and can be well matched with the IVUS.

Drug release study

Under conditions characterised by vascular injury, hypoxia, and shear stress alterations, the expression of miR-126-3p in endothelial cells is enhanced. This upregulation subsequently leads to the downregulation of sprouty-related EVH1 domain-containing protein 1 (SPRED1) and phosphoinositol-3 kinase regulatory subunit 2 (PI3KR2). Consequently, the downstream recombinant c-raf proto-oncogene serine/threonine protein kinase (RAF1)/extracellular regulated protein kinase (ERK) pathway and phosphatidylinositol 3-kinase (PI3K)/

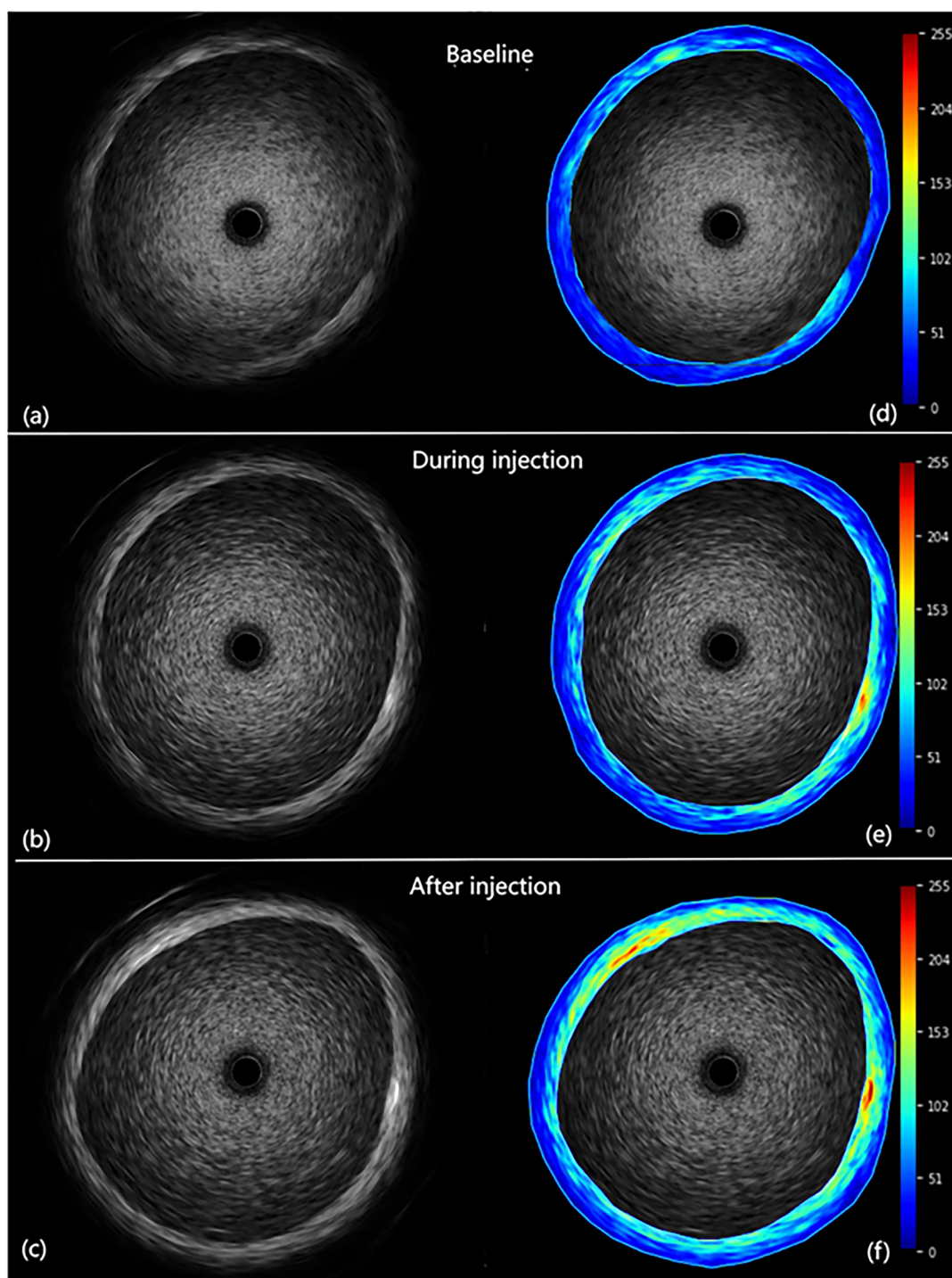


Figure 7. Depiction of qualitative representation of enhancement. Unprocessed images are displayed (a) before, (b) during, and (c) after injection of PBCA NPs. Corresponding processed images are displayed in (d–f). Enhancement is graded from minimal (blue) to maximal (red). Values are a percentage of the maximum grey level intensity difference.

Table 1. Depiction of quantitative representation of enhancement.

| | Area (px ²) | Mean | StdDev | Mode | Min | Max |
|------------------|-------------------------|--------|--------|------|-----|-----|
| After injection | 3.326 | 78.075 | 38.480 | 43 | 0 | 253 |
| During injection | 3.178 | 58.427 | 32.321 | 44 | 0 | 228 |
| Baseline | 2.972 | 39.912 | 22.957 | 31 | 0 | 150 |

protein kinase B (AKT) pathway are activated, thereby facilitating the activation of the vascular endothelial growth factor (VEGF) signalling pathway. This activation ultimately promotes

angiogenesis. In contrast, downregulation of miR-126-3p can cause the upregulation of SPRED1 and PI3KR2, and then inhibit the downstream RAF1/ERK pathway and PI3K/AKT pathway respectively, thereby inhibiting VEGF signalling pathway, leading to the obstruction of angiogenesis [30–35].

This study observed a decrease in the expression levels of SPRED1 and PI3KR2 in the model group (rat aortic endothelial cell injury model) when compared to the control group. In comparison to the model group, the therapy group (treated with the ant-miR-126 loaded PBCA NPs) exhibited

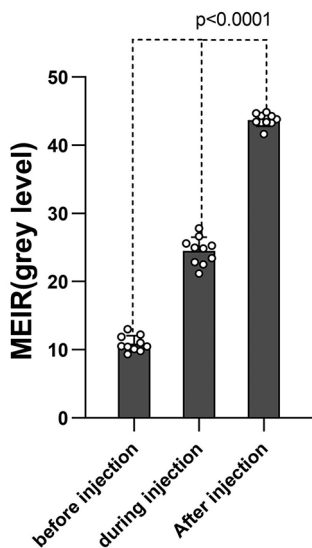


Figure 8. The mean enhancement in region of interest (MEIR) after PBCA NPs injection in the vascular wall regions.

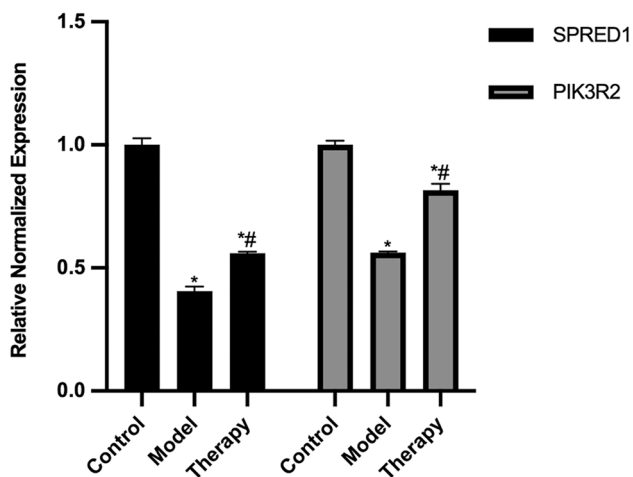


Figure 9. Relative expression of SPRED1 and PI3KR2 in each group. The control group was performed on normal rat aortic endothelial cells, the model group was performed on a rat aortic endothelial cell injury model, and the treatment group was treated with the addition of the ant-miR-126 loaded PBCA NPs to the rat aortic endothelial cell injury model. * indicates $p < .05$ compared with the control group, # indicates $p < .05$ compared with the model group.

upregulation of SPRED1 and PI3KR2. Following cellular injury, miR-126 was upregulated in the model group, resulting in the downregulation of downstream SPRED1 and PI3KR2. The therapy group inhibited miR-126, so the downstream SPRED1 and PI3KR2 were higher than those in the model group (Figure 9). Given the inherent limitations in directly detecting the presence of loaded ant-miR-126, our ability to establish its release and subsequent functional impact is contingent upon observing the resultant alterations in downstream molecular processes. Furthermore, the elucidation and clarification of the treatment effect and specific mechanism of action are yet to be revealed and explicated by a substantial body of pertinent research.

According to the above research findings, it is posited that the PBCA NPs can be used in combination with IVUS for simultaneous diagnosis and targeted therapy of coronary

atherosclerosis. The force generated on the NPs is due to the absorption of ultrasound momentum, called the ultrasound radiation force. In the absence of this force, NPs in laminar flow exhibit lateral migration towards the vessel axis, which prevents NPs from contacting the endothelium [36]. However, the ultrasound radiation force is able to propel the flowing NPs into contact with the vessel wall, where they enter the vascular layer through the endothelial gap [13]. Therefore, the drug-loaded PBCA NPs can accumulate at the periphery of blood vessels, and penetrate into the lesion through the endothelial clefts in the affected area, by the ultrasonic radiation force from IVUS. Subsequently, the PBCA NPs can be naturally hydrolysed, release the internal drugs and achieve targeted drug delivery (Figure 10). miR-126 is located on chromosome 9 with a length of 85 nt and is the most abundant miRNA expressed in vascular endothelial cells. At present, many studies have shown that it is positively correlated with the formation of new nutrient vessels and the progression of coronary heart disease [37]. Simultaneously, it is also abundantly expressed in platelets, plays a key role in the process of platelet activation, and exhibits an inverse relationship with platelet inhibition. Therefore, the current accumulating evidence shows that miR-126 may be used as a potential new therapeutic target to inhibit the formation of new nutrient vessels, delay or even reverse the progression of coronary heart disease, and inhibit the function of platelets [38, 39]. The ant-miR-126 used in this study inhibits the function of miR-126 through strong competitive binding with the mature miR-126 in vivo, preventing the complementary pairing of miR-126 and its target gene mRNA, so as to achieve the therapeutic purpose.

Conclusions and recommendations

In this study, polymeric nanoparticles, PBCA NPs, were synthesised using butyl cyanoacrylate as monomer in a suspension polymerisation scheme. By adjusting the parameters during the manufacturing process, the NPs compatible with the use of IVUS were successfully optimised. These NPs are ideal as empty drug carriers.

The resultant nanoparticle drug carrier exhibited spherical particles with hollow centres, with an average diameter of 216 nm. The NPs possessed a stable negative surface potential of -22.2 mV. In vitro experiments suggest that these NPs are non-toxic, stable, and compatible with the high-frequency probe of IVUS. By enhancing ultrasound signals, they effectively enhance the resolution of IVUS. Under the radiation force of IVUS, these NPs can pass through gaps in the vascular endothelium of lesions, concentrate at the margins, penetrate the lesion, and eventually decompose naturally, releasing the encapsulated drugs. In this way, an IVUS-PBCA NPs targeted drug delivery system is created.

In this study, ant-miR-126-loaded PBCA NPs were further prepared. These drug-loaded NPs share similar physicochemical properties with the blank carrier, demonstrate safety and stability, and have been shown to successfully release the encapsulated ant-miR-126 *in vitro*. This release further suppresses the expression of cellular miR-126, enabling gene

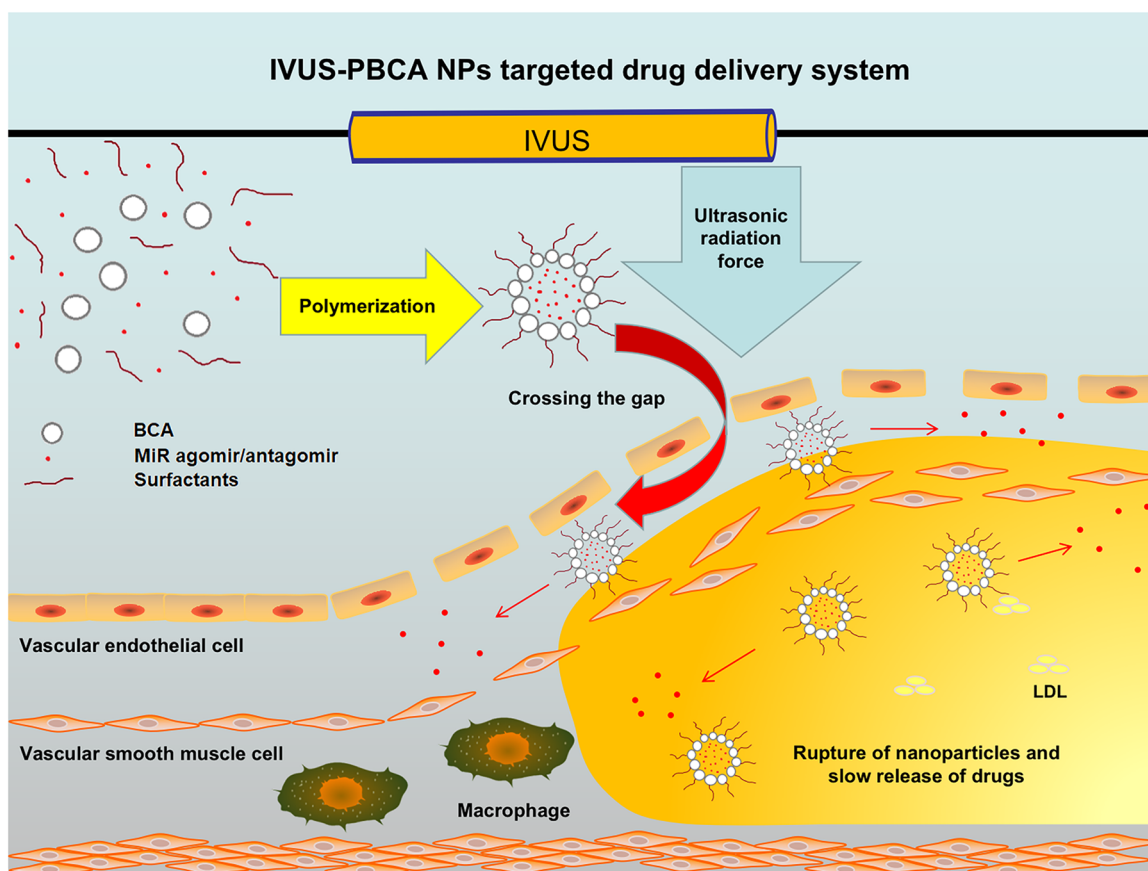


Figure 10. Schematic diagram of intravascular ultrasound (IVUS)-PBCA NPs targeted drug delivery system. Abbreviations: LDL, low density lipoprotein.

regulation that influences a series of downstream proteins and triggers their effects. In combination with IVUS in the future, targeted gene regulation can be achieved.

Future work involves further *in vivo* experimentation, potentially using experimental pigs as test subjects for modelling vulnerable coronary artery plaques. Through comparative experiments, the IVUS-PBCA NPs targeted drug delivery system will be applied for targeted gene regulation. The expression of target genes and changes in protein molecules within downstream pathways will be monitored. This approach aims to achieve simultaneous diagnosis and targeted therapy of coronary atherosclerosis.

Acknowledgments

Not applicable.

Disclosure statement

No potential conflict of interest was reported by the author(s).

Author contributions

Congying Wang: Conceptualisation, Methodology, Writing – Original draft, Implementation research, Data acquisition, processing, and analysis; Haodong Jiang: Data visualisation, Writing – Original draft, Implementation research, Data acquisition, processing, and analysis; Jia Zhu: Experimental assistance, Data analysis, Validation, Data visualisation; Yunpeng Jin:

Conceptualisation, Experimental guidance, Writing – review & editing, Supervision, Resources. All authors read and approved the final version of the manuscript.

Funding

This study was funded by the Foundation of Zhejiang Provincial Education Department (Grant No. Y202249328), Foundation of The fourth Affiliated Hospital Zhejiang University School of Medicine (Grant No. JG20230203). The funders had no role in the study design, data collection and analysis, the decision to publish or the preparation of the manuscript.

ORCID

Congying Wang  <http://orcid.org/0000-0001-6374-032X>
Yunpeng Jin  <http://orcid.org/0000-0003-4242-7072>

Data availability statement

The data that support the findings of this study are available from the corresponding author, Yunpeng Jin, upon reasonable request.

References

- [1] Finn AV, Nakano M, Narula J, et al. Concept of vulnerable/unstable plaque. *Arterioscler Thromb Vasc Biol.* 2010;30(7):1282–1292. doi: [10.1161/ATVBAHA.108.179739](https://doi.org/10.1161/ATVBAHA.108.179739).
- [2] Peng C, Wu H, Kim S, et al. Recent advances in transducers for intravascular ultrasound (IVUS) imaging. *Sensors (Basel).* 2021;21(10):3540. doi: [10.3390/s21103540](https://doi.org/10.3390/s21103540).

- [3] Goertz DE, Frijlink ME, de Jong N, et al. Nonlinear intravascular ultrasound contrast imaging. *Ultrasound Med Biol*. 2006;32(4):491–502. doi: [10.1016/j.ultrasmedbio.2006.01.001](https://doi.org/10.1016/j.ultrasmedbio.2006.01.001).
- [4] Goertz DE, Frijlink ME, Tempel D, et al. Contrast harmonic intravascular ultrasound: a feasibility study for vasa vasorum imaging. *Invest Radiol*. 2006;41(8):631–638. doi: [10.1097/01.rli.0000229773.11715.da](https://doi.org/10.1097/01.rli.0000229773.11715.da).
- [5] Vavuranakis M, Kakadiaris IA, O'Malley SM, et al. A new method for assessment of plaque vulnerability based on vasa vasorum imaging, by using contrast-enhanced intravascular ultrasound and differential image analysis. *Int J Cardiol*. 2008;130(1):23–29. doi: [10.1016/j.ijcard.2007.07.170](https://doi.org/10.1016/j.ijcard.2007.07.170).
- [6] Shekhar H, Huntzicker S, Awuor I, et al. Chirp-coded ultraharmonic imaging with a modified clinical intravascular ultrasound system. *Ultrason Imaging*. 2016;38(6):403–419. doi: [10.1177/0161734615618639](https://doi.org/10.1177/0161734615618639).
- [7] Ferrara K, Pollard R, Borden M. Ultrasound microbubble contrast agents: fundamentals and application to gene and drug delivery. *Annu Rev Biomed Eng*. 2007;9(1):415–447. doi: [10.1146/annurev.bioeng.8.061505.095852](https://doi.org/10.1146/annurev.bioeng.8.061505.095852).
- [8] Unger EC, Porter T, Culp W, et al. Therapeutic applications of lipid-coated microbubbles. *Adv Drug Deliv Rev*. 2004;56(9):1291–1314. doi: [10.1016/j.addr.2003.12.006](https://doi.org/10.1016/j.addr.2003.12.006).
- [9] Dixon AJ, Kilroy JP, Dhanaliwala AH, et al. Microbubble-mediated intravascular ultrasound imaging and drug delivery. *IEEE Trans Ultrason Ferroelectr Freq Control*. 2015;62(9):1674–1685. doi: [10.1109/TUFFC.2015.007143](https://doi.org/10.1109/TUFFC.2015.007143).
- [10] Doinikov AA, Haac JF, Dayton PA. Resonance frequencies of lipid-shelled microbubbles in the regime of nonlinear oscillations. *Ultrasonics*. 2009;49(2):263–268. doi: [10.1016/j.ultras.2008.09.006](https://doi.org/10.1016/j.ultras.2008.09.006).
- [11] Lindsey BD, Martin KH, Jiang X, et al. Adaptive windowing in contrast-enhanced intravascular ultrasound imaging. *Ultrasonics*. 2016;70:123–135. doi: [10.1016/j.ultras.2016.04.022](https://doi.org/10.1016/j.ultras.2016.04.022).
- [12] Schneider M. Design of an ultrasound contrast agent for myocardial perfusion. *Echocardiography*. 2000;17(6Pt 2):S11–S6. doi: [10.1111/j.1540-8175.2000.tb01189.x](https://doi.org/10.1111/j.1540-8175.2000.tb01189.x).
- [13] Zhao S, Borden M, Bloch SH, et al. Radiation-force assisted targeting facilitates ultrasonic molecular imaging. *Mol Imaging*. 2004;3(3):135–148. doi: [10.1162/15353500200404115](https://doi.org/10.1162/15353500200404115).
- [14] Nicolas J, Couvreur P. Synthesis of poly(alkyl cyanoacrylate)-based colloidal nanomedicines. *Wiley Interdiscip Rev Nanomed Nanobiotechnol*. 2009;1(1):111–127. doi: [10.1002/wnan.15](https://doi.org/10.1002/wnan.15).
- [15] Shi-Ya G, Min X, Zhi-Peng C, et al. Application of polybutylcyanoacrylate nanoparticles in drug delivery systems. *Chin J New Drugs*. 2013;22(11):1278–1284.
- [16] Le MN, Nguyen TA. Innovative microRNA quantification by qPCR. *Mol Ther Nucleic Acids*. 2023;31:628–630. doi: [10.1016/j.omtn.2023.02.012](https://doi.org/10.1016/j.omtn.2023.02.012).
- [17] Tabatabaei MS, Ahmed M. Enzyme-linked immunosorbent assay (ELISA). *Methods Mol Biol*. 2022;2508:115–134. doi: [10.1007/978-1-0716-2376-3_10](https://doi.org/10.1007/978-1-0716-2376-3_10).
- [18] Ćurić A, Möschwitzer JP, Fricker G. Development and characterization of novel highly-loaded itraconazole poly(butyl cyanoacrylate) polymeric nanoparticles. *Eur J Pharm Biopharm*. 2017;114:175–185. doi: [10.1016/j.ejpb.2017.01.014](https://doi.org/10.1016/j.ejpb.2017.01.014).
- [19] Krishnamoorthy B, Karanam V, Chellan VR, et al. Polymersomes as an effective drug delivery system for glioma—a review. *J Drug Target*. 2014;22(6):469–477. doi: [10.3109/1061186X.2014.916712](https://doi.org/10.3109/1061186X.2014.916712).
- [20] Mousavi SV, Hashemianzadeh SM. Poly (n-butyl cyanoacrylate) as a nanocarrier for rivastigmine transport across the blood-brain barrier in alzheimer's disease treatment: a perspective from molecular dynamics simulations. *J Mol Model*. 2018;24(9):252. doi: [10.1007/s00894-018-3799-0](https://doi.org/10.1007/s00894-018-3799-0).
- [21] Zheng L, Shen L, Li Z, et al. Design, preparation, and evaluation of osthonol poly-butyl-cyanoacrylate nanoparticles with improved in vitro anticancer activity in neuroblastoma treatment. *Molecules*. 2022;27(20):6908. doi: [10.3390/molecules27206908](https://doi.org/10.3390/molecules27206908).
- [22] Lenaerts V, Couvreur P, Christiaens-Leyh D, et al. Degradation of poly (isobutyl cyanoacrylate) nanoparticles. *Biomaterials*. 1984;5(2):65–68. doi: [10.1016/0142-9612\(84\)90002-4](https://doi.org/10.1016/0142-9612(84)90002-4).
- [23] Casertari L, Villasaliu D, Castagnino E, et al. PEGylated chitosan derivatives: synthesis, characterizations and pharmaceutical applications. *Prog Polym Sci*. 2012;37(5):659–685. doi: [10.1016/j.progpolymsci.2011.10.001](https://doi.org/10.1016/j.progpolymsci.2011.10.001).
- [24] Bagherpour Doun SK, Alavi SE, Koohi Mofatkhari Esfahani M, et al. Efficacy of cisplatin-loaded poly butyl cyanoacrylate nanoparticles on the ovarian cancer: an in vitro study. *Tumour Biol*. 2014;35(8):7491–7497. doi: [10.1007/s13277-014-1996-8](https://doi.org/10.1007/s13277-014-1996-8).
- [25] Gabisonia K, Prosdocimo G, Aquaro GD, et al. MicroRNA therapy stimulates uncontrolled cardiac repair after myocardial infarction in pigs. *Nature*. 2019;569(7756):418–422. doi: [10.1038/s41586-019-1191-6](https://doi.org/10.1038/s41586-019-1191-6).
- [26] Huang CK, Kafert-Kasting S, Thum T. Preclinical and clinical development of noncoding RNA therapeutics for cardiovascular disease. *Circ Res*. 2020;126(5):663–678. doi: [10.1161/CIRCRESAHA.119.315856](https://doi.org/10.1161/CIRCRESAHA.119.315856).
- [27] Ginckels P, Holvoet P. Oxidative stress and inflammation in cardiovascular diseases and cancer: role of non-coding RNAs. *Yale J Biol Med*. 2022;95(1):129–152.
- [28] Ma J, Martin K, Dayton PA, et al. A preliminary engineering design of intravascular dual-frequency transducers for contrast-enhanced acoustic angiography and molecular imaging. *IEEE Trans Ultrason Ferroelectr Freq Contr*. 2014;61(5):870–880. doi: [10.1109/TUFFC.2014.2977](https://doi.org/10.1109/TUFFC.2014.2977).
- [29] Li Y, Ma J, Martin KH, et al. An integrated system for superharmonic contrast-enhanced ultrasound imaging: design and intravascular phantom imaging study. *IEEE Trans Biomed Eng*. 2016;63(9):1933–1943. doi: [10.1109/TBME.2015.2506639](https://doi.org/10.1109/TBME.2015.2506639).
- [30] Bassand K, Metzinger L, Naim M, et al. miR-126-3p is essential for CXCL12-induced angiogenesis. *J Cell Mol Med*. 2021;25(13):6032–6045. doi: [10.1111/jcmm.16460](https://doi.org/10.1111/jcmm.16460).
- [31] Hao XZ, Fan HM. Identification of miRNAs as atherosclerosis biomarkers and functional role of miR-126 in atherosclerosis progression through MAPK signalling pathway. *Eur Rev Med Pharmacol Sci*. 2017;21(11):2725–2733.
- [32] Moghaddam AS, Afshari JT, Esmaeili SA, et al. Cardioprotective microRNAs: lessons from stem cell-derived exosomal microRNAs to treat cardiovascular disease. *Atherosclerosis*. 2019;285:1–9. doi: [10.1016/j.atherosclerosis.2019.03.016](https://doi.org/10.1016/j.atherosclerosis.2019.03.016).
- [33] Tao SC, Guo SC, Li M, et al. Chitosan wound dressings incorporating exosomes derived from MicroRNA-126-overexpressing synovium mesenchymal stem cells provide sustained release of exosomes and heal full-thickness skin defects in a diabetic rat model. *Stem Cells Transl Med*. 2017;6(3):736–747. doi: [10.5966/sctm.2016-0275](https://doi.org/10.5966/sctm.2016-0275).
- [34] Zhang J, Sun XJ, Chen J, et al. Increasing the miR-126 expression in the peripheral blood of patients with diabetic foot ulcers treated with maggot debridement therapy. *J Diabet Compl*. 2017;31(1):241–244. doi: [10.1016/j.jdiacomp.2016.07.026](https://doi.org/10.1016/j.jdiacomp.2016.07.026).
- [35] Zhou Z, Schober A, Nazari-Jahantigh M. Dicer promotes endothelial recovery and limits lesion formation after vascular injury through miR-126-5p. *Int J Cardiol*. 2018;273:199–202. doi: [10.1016/j.ijcard.2018.09.006](https://doi.org/10.1016/j.ijcard.2018.09.006).
- [36] Rychak JJ, Klibanov AL, Ley KF, et al. Enhanced targeting of ultrasound contrast agents using acoustic radiation force. *Ultrasound Med Biol*. 2007;33(7):1132–1139. doi: [10.1016/j.ultrasmedbio.2007.01.005](https://doi.org/10.1016/j.ultrasmedbio.2007.01.005).
- [37] Jansen F, Yang X, Hoelscher M, et al. Endothelial microparticle-mediated transfer of MicroRNA-126 promotes vascular endothelial cell repair via SPRED1 and is abrogated in glucose-damaged endothelial microparticles. *Circulation*. 2013;128(18):2026–2038. doi: [10.1161/CIRCULATIONAHA.113.001720](https://doi.org/10.1161/CIRCULATIONAHA.113.001720).
- [38] Jansen F, Yang X, Proebsting S, et al. MicroRNA expression in circulating microvesicles predicts cardiovascular events in patients with coronary artery disease. *J Am Heart Assoc*. 2014;3(6):e001249. doi: [10.1161/JAHA.114.001249](https://doi.org/10.1161/JAHA.114.001249).
- [39] Pordzik J, Pisarz K, De Rosa S, et al. The potential role of platelet-related microRNAs in the development of cardiovascular events in high-risk populations, including diabetic patients: a review. *Front Endocrinol (Lausanne)*. 2018;9:74. doi: [10.3389/fendo.2018.00074](https://doi.org/10.3389/fendo.2018.00074).